Cooperative Adsorption of Ezrin on PIP_2-Containing Membranes†

Alexander Herrig,‡ Matthias Janke,§ Judith Austermann,|| Volker Gerke,|| Andreas Janshoff,§ and Claudia Steinem*,‡

Institut für Organische und Biomolekulare Chemie, Georg-August-Universität, Tammannstrasse 2, 37077 Göttingen, Germany, Institut für Physikalische Chemie, Johannes-Gutenberg-Universität, Welder Weg 11, 55128 Mainz, Germany, and Institut für Medizinische Biochemie, Westfälische Wilhelms-Universität, von-Esmarch-Strasse 56, 48149 Münster, Germany

Received May 29, 2006; Revised Manuscript Received August 21, 2006

ABSTRACT: By means of the quartz crystal microbalance (QCM) and scanning force microscopy (SFM), the adsorption of ezrin, a member of the ezrin/radixin/moesin protein family, on L-α-phosphatidylinositol-4,5-bisphosphate (PIP_2) containing solid-supported membranes was investigated. An increase in the PIP_2 content in 1-palmitoyl-2-oleoyl-*sn*-glycero-3-phosphocholine (POPC) membranes resulted in an increased amount of bound ezrin strongly supporting the crucial role of PIP_2 for ezrin recruitment to membranes. No ezrin adsorption to membranes composed of pure POPC was detected. To characterize the binding process in more detail, the kinetics and reversibility of ezrin adsorption were investigated by the QCM technique, showing that the protein remains partly bound after rinsing with pure buffer, which we suspected to be a result of lateral interactions between the proteins. SFM images revealed the formation of two-dimensional ezrin clusters on PIP_2-doped POPC membranes. Time-elapsed SFM images show that the growth of protein domains occurs from a few nucleation sites. The QCM data in conjunction with the results obtained by SFM led us to propose that the binding process of ezrin occurs in a positive cooperative manner. When lateral interactions of the proteins on the membrane were taken into account, we were able to simulate the kinetics obtained from time-resolved QCM readouts by employing a model developed by Minton. On the basis of the kinetic analysis, we were also able to reconstruct the adsorption isotherm.

The plasma membrane−cytoskeleton interface is a dynamic structure, participating in a variety of cellular events. Nevertheless, only a few proteins have been identified that provide a direct link between components of the cytoskeleton and the plasma membrane. Among these, the ezrin/radixin/moesin (ERM)[1] family of proteins functions as membrane−cytoskeleton linkers, thereby determining cell shape and motility, participating in signal-transduction pathways, and regulating the connection between membrane proteins and the cytoskeleton (*1*−*4*). Characteristically, proteins of the ERM family are organized in two distinct domains, called N-terminal ERM association domain (N-ERMAD) and C-terminal ERM association domain (C-ERMAD). The C-terminal domain of ERM proteins harbors a F-actin-binding site consisting of 34 amino acids, which are highly conserved in the protein family (*5*), whereas the N-terminal domain mediates the binding to membrane proteins and lipids.

Ezrin, a member of the ERM protein family, was first isolated and purified as a cytoskeletal component of intestinal microvilli (*6*). It consists of the N-ERMAD, followed by a predicted α-helical region, which is thought to have a high potential to form coiled-coil structures, and terminates in the C-ERMAD (*7*). The binding of ezrin to membrane proteins occurs in either an indirect manner mediated by scaffolding proteins such as ERM-binding phosphoprotein 50 (EBP50) (*8*) or directly as observed for the receptor for hyaluronate, CD44 (*9*−*11*), and for intercellular adhesion molecule-2 (ICAM-2) (*10*, *12*). Moreover, a direct interaction of ezrin with lipid bilayers containing L-α-phosphatidylinositol-4,5-bisphosphate (PIP_2) has been reported (*13*−*15*), and the presence of PIP_2 seems to facilitate the binding of ezrin to membrane proteins (*14*, *16*). Although not very abundant in membranes, PIP_2 fulfils important roles in regulating membrane trafficking, membrane−cytoskeleton linkage, and several cell-signaling events (*17*−*20*). In general, the binding of PIP_2 to proteins is mediated by certain domains, of which the pleckstrin homology (PH), the epsin N-terminal homology (ENTH), and the 4.1 and ERM (FERM) domains are the best characterized ones (*20*). Ezrin contains a binding site for PIP_2 that is localized in its N-terminal domain. It has been shown that the association of ezrin with PIP_2-containing vesicles can be almost completely abolished by

† This work was supported in part by a grant from the Deutsche Forschungsgemeinschaft to V.G. (Ge 514/5-1). Financial support by the Deutsche Forschungsgemeinschaft (SFB 625) to A.J. is gratefully acknowledged.

* To whom correspondence should be addressed. Telephone: +49-(551)-393294. Fax: +49-(551)-393228. E-mail: claudia.steinem@chemie.uni-goettingen.de.

‡ Georg-August-Universität.

§ Johannes-Gutenberg-Universität.

|| Westfälische Wilhelms-Universität.

[1] Abbreviations: C-ERMAD, C-terminal ERM association domain; DC, direct current; DTT, dithiothreitol; EBP50, ERM-binding phosphoprotein of 50 kDa; EDTA, ethylenediaminetetraacetic acid; EGF, epidermal growth factor; ENTH, epsin N-terminal homology; ERM, ezrin/radixin/moesin; FERM, 4.1 and ERM; ICAM-2, intercellular adhesion molecule 2; LUV, large unilamellar vesicle; MLV, multilamellar vesicle; N-ERMAD, N-terminal ERM association domain; Ni−NTA, Ni−nitrilotriacetic acid; PAGE, polyacrylamide gel electrophoresis; PH, pleckstrin homology; PIP_2, L-α-phosphatidylinositol-4,5-bisphosphate; PMSF, phenylmethylsulfonylfluoride; POPC, 1-palmitoyl-2-oleoyl-*sn*-glycero-3-phosphocholine; QCM, quartz crystal microbalance; SDS, sodium dodecyl sulfate; SFM, scanning force microscopy.

10.1021/bi061064a CCC: $33.50
Published on Web 10/05/2006

mutagenesis of the PIP_2-binding motifs (*21*). Furthermore, under physiological conditions, ezrin discriminates between PIP_2, phosphatidylinositol-4-monophosphate, phosphatidylinositol, and phosphatidylserine (*13*). In light of these findings, PIP_2 emerges as a determinant for the conformational activation process of ezrin (*15*). In monomeric ezrin, N-ERMAD and C-ERMAD are tightly associated, thus leaving ezrin in an inactive, so-called dormant state, in which the F-actin- and membrane-binding sites are usually masked. The activation of ezrin can occur upon threonine phosphorylation in the C-terminal domain, resulting in a conformational change of the protein (*1*, *22*, *23*). Recently, an alternative pathway of activating ezrin has been proposed on the basis of the finding that the interaction of S100P with ezrin can at least partially activate ezrin in a Ca^{2+}-dependent manner (*24*).

In this study, we investigated in detail the interaction of ezrin with solid-supported membranes containing PIP_2. In particular, the influence of the PIP_2 content in the membrane upon ezrin binding and its reversibility was analyzed by means of the quartz crystal microbalance, which allows for the determination of thermodynamic and kinetic parameters in a label-free fashion because of the correspondence of the frequency change to the number of adsorbed molecules (*25*, *26*). Brisson and co-workers (*27*−*30*) have shown that a combination of the quartz crystal microbalance (QCM) and scanning force microscopy (SFM) (*31*, *32*) allows for a detailed analysis of the formation process of lipid bilayers and protein adsorption on lipid membranes. We used a combination of QCM and SFM to elucidate the interaction of ezrin to PIP_2-containing membranes, suggesting a positive cooperative binding.

EXPERIMENTAL PROCEDURES

Materials. The phospholipids 1-palmitoyl-2-oleoyl-*sn*-glycero-3-phosphocholine (POPC) and PIP_2 were purchased from Avanti Polar Lipids (Alabaster, AL). The 5 MHz overtone polished AT-cut quartz crystals (plano-plano) were from KVG (Neckarbischofsheim, Germany). Gold used for the working electrodes was obtained from Cressington (Valencia, PA). Silicon wafers were from Silicon Materials (Landsberg, Germany). All chemicals were of the highest purity available. Water was purified first through a Millipore water purification system Milli-RO 3 plus and finally with a Millipore ultrapure water system Milli-Q plus 185 (specific resistance = 18.2 MΩ/cm) (Billerica, MA).

Protein Purification. Recombinant expression and purification of ezrin is described in detail elsewhere (*24*). Briefly, transformed *Escherichia coli* cells [strain BL21(DE3)pLysS] containing the bacterial expression vector pET 28a+ (Novagen) encoding wild-type ezrin with an N-terminal histidine tag were grown to an OD_{600} of 0.6. Recombinant protein expression was induced by adding isopropyl-β-D-thiogalactopyranoside to a concentration of 1 mM. After 3 h, cells were harvested by centrifugation (5000*g* for 10 min at 4 °C) and resuspended in lysis buffer [50 mM Tris/HCl, 20 mM imidazole/HCl, 300 mM NaCl, 1 mM ethylenediaminetetraacetic acid (EDTA), 10 mM β-mercaptoethanol, 1 mM phenylmethylsulfonylfluoride (PMSF), and 10 μM leupeptin at pH 7.5]. Subsequently, the cells were lysed by sonication. The lysates were centrifuged for 1 h and 100000*g* at 4 °C, and the supernatant was applied to a Ni−nitrilotriacetic acid (Ni−NTA) agarose column (Qiagen, Hilden, Germany) equilibrated in lysis buffer. The column was washed twice with lysis buffer containing 25 mM imidazole/HCl at pH 7.5 and 35 mM imidazole/HCl at pH 7.5, respectively. Ezrin was eluted with 300 mM imidazole/HCl, 10 mM β-mercaptoethanol, and 1 mM PMSF at pH 7.5 and stored at 4 °C.

Vesicle Preparation. Mixed lipid films composed of POPC [10 mg/mL in chlorofom/methanol (1:1)] doped with various amounts of PIP_2 [1 mg/mL in chloroform/methanol/water (8:1:1)] were prepared under a stream of nitrogen followed by 3 h under vacuum at 35 °C and stored at 4 °C. Multilamellar vesicles (MLVs) were formed by first swelling the lipid films in buffer solution (20 mM Tris/HCl, 50 mM KCl, 0.1 mM EDTA, and 1 mM NaN_3 at pH 7.4) for 30 min followed by vortexing them 3 times for 30 s every 5 min. Large unilamellar vesicles (LUVs) were produced from MLVs by pressing them through a polycarbonate membrane with 100 nm pore diameters using a miniextruder (Liposo-Fast, Avestin, Canada).

Vesicle Co-sedimentation Assay. Prior to the experiments, ezrin was dialyzed against 20 mM Tris/HCl, 50 mM KCl, 0.1 mM EDTA, and 1 mM NaN_3 at pH 7.4 followed by determination of the protein concentration (*33*). Freshly prepared MLVs were incubated with ezrin for 20 min at 20 °C. Final concentrations were 1.4 μM (protein) and 0.5 mg/mL (lipid). MLVs were centrifuged at 4 °C and 15000*g* for 20 min. A sample was taken from the supernatant. Subsequently, the supernatant was carefully removed, and the pellet was washed with buffer solution to remove nonspecifically bound protein followed by a centrifugation for 20 min at 15000*g* and 4 °C. Samples were again taken from the supernatant and pellet. For sodium dodecyl sulfate−polyacrylamide gel electrophoresis (SDS−PAGE) analysis, all samples were treated with 0.175 M Tris/HCl, 5% SDS (w/v), 15% glycerol (v/v), 0.06 g/L bromphenol blue, and 0.3 M dithiothreitol (DTT) at pH 6.8 and heated for 5 min at 100 °C, and equivalent amounts of pellet and supernatant fractions were then analyzed in 12.5% SDS−polyacrylamide gels stained with Coomassie Brillant Blue (*34*).

QCM. To investigate lipid protein interactions, the QCM was used in the active mode as described elsewhere (*35*). In brief, an AT-cut quartz plate with a 5 MHz fundamental resonance frequency was mounted in a fluid cell made of Teflon in such that the solid-supported membrane was exposed to the aqueous solution. Spring contacts were connected to the gold electrodes of the quartz plate with an oscillator circuit (TTL SN74LS124N, Texas Instruments, TX), which was driven by a power supply (E3630A, Agilent Technologies, CA) at 4 V direct current (DC) voltage. The change in frequency of the quartz resonator was recorded using a frequency counter (53181A, Agilent Technologies, CA) connected to a computer. Supplied with an inlet and an outlet connecting the Teflon cell to a peristaltic pump, the setup allows for the addition of the protein solution from outside the cell. The entire system was placed in a water-jacketed Faraday cage thermostated at 20 °C.

Preparation of Solid-Supported Bilayers on Gold. Prior to use, the gold electrodes (0.25 cm^2) of a 5 MHz AT-cut quartz plate (14 mm in diameter) were cleaned in argon plasma (Plasma cleaner, Harrick, NY) for 5 min. The quartz

plate was mounted into a Teflon cell, and one side was exposed to a 1 mM ethanolic octanethiol solution for 1 h. Subsequently, the gold surface was rinsed first with ethanol and then with buffer solution (20 mM Tris/HCl, 50 mM KCl, 0.1 mM EDTA, and 1 mM NaN_3 at pH 7.4) to remove nonbound octanethiol. The completeness of the self-assembled monolayer was monitored by impedance spectroscopy (Solartron Instruments, Farnborough, U.K.). A capacitance of 2.0 ± 0.2 μF/cm^2 indicated a successful chemisorption. The formation of the second monolayer composed of POPC and PIP_2 was achieved by incubation of the octanethiol monolayer with LUVs (0.5 mg/mL) for 1 h at room temperature to induce fusion of the vesicles on the hydrophobic monolayer. The quality of the resulting solid-supported bilayer was analyzed by impedance spectroscopy. Capacitance values of 1.1 ± 0.2 μF/cm^2 confirmed a successful preparation of bilayers. The remaining vesicles were removed by rinsing the cell with pure buffer solution.

SFM. Measurements were carried out with a commercial scanning force microscope (Dimension 3100 with Nanoscope IIIa A/D controller, Veeco Instruments, Santa Barbara, CA) and Si_3N_4 cantilevers (OMCL-TR 400 PSA, Olympus, Japan). All topographs were measured in TappingMode in liquids with a scan speed according to the scan size, about 1−2 lines per second (frame size, 3−40 μm).

Preparation of Solid-Supported Membranes on Silicon Dioxide. First, silicon (0.5 × 1.5 cm^2) was thoroughly cleaned with isopropanol and water and then placed in an aqueous solution of 1% (v/v) HF at room temperature for 15 min to remove the native silicon oxide layer. After the hydrophobic silicon was intensively rinsed with water, it was incubated in an aqueous solution of NH_3 and H_2O_2 (5:1:1 water/NH_3/H_2O_2) at 70 °C for 15 min to produce a newly grown thin hydrophilic silicon oxide layer. Immediately after rinsing with water, these silicon substrates were mounted in a sample holder and incubated with the vesicle suspension. If the substrates were not immediately used, they were stored under water for a maximum of a week and treated with an oxygen plasma for 10 min prior use.

Prior to the addition of a suspension of LUVs (0.3 mg/mL) in 20 mM Tris/HCl, 50 mM KCl, and 0.1 mM EDTA at pH 7.4 to the hydrophilic silicon surface, $CaCl_2$ (2 mM) was added to the suspension to increase the adhesion and spreading of the vesicles to the surface. The silicon surfaces were incubated for 1−2 h and subsequently rinsed with buffer solution containing 15 mM EDTA, followed by rinsing with 20 mM Tris/HCl, 50 mM KCl, and 0.1 mM EDTA at pH 7.4.

RESULTS

Interaction of Ezrin with Vesicles Containing Different Amounts of PIP_2. Among other properties, ezrin is known to interact with PIP_2 via its N-terminal domain (*13*, *21*). To first characterize the interaction of ezrin with PIP_2, vesicle co-sedimentation assays were performed with MLVs composed of POPC and various amounts of PIP_2. Figure 1 reveals that ezrin is more efficiently sequestered into the liposome pellet when the PIP_2 content exceeded 3 mol %. The interaction is specific because pure POPC vesicles did not bind ezrin in the co-sedimentation assay (data not shown).

Interaction of Ezrin with Solid-Supported Membranes Containing Different Amounts of PIP_2. To elucidate the influence of the PIP_2 concentration on ezrin adsorption on a membrane in more detail, binding was recorded quantitatively by the QCM technique, while the molecular organization was visualized by SFM. For QCM measurements, we used 5 MHz quartz plates with solid-supported membranes composed of an octanethiol monolayer and a second phospholipid monolayer of either pure POPC or POPC doped with various amounts of PIP_2. Figure 2A shows typical time courses of frequency shifts of the quartz plate upon the addition of 0.1 μM ezrin in 20 mM Tris/HCl, 50 mM KCl, 0.1 mM EDTA, and 1 mM NaN_3 at pH 7.4. The decrease in resonance frequency is proportional to the amount of adsorbed ezrin on the lipid layer. Δf is defined as the difference between the actual resonance frequency $f(t)$ and $f(t = 0)$. The largest ezrin coverage of the membrane

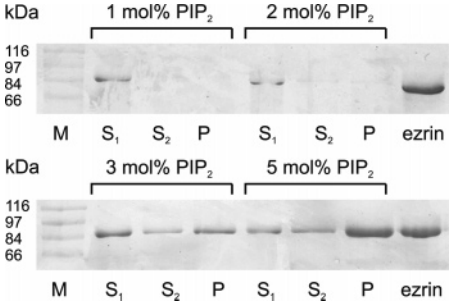

FIGURE 1: SDS−PAGE analysis of the co-sedimentation of ezrin (1.4 μM) with MLVs (0.5 mg/mL) consisting of POPC doped with PIP_2 as indicated. The vesicle assays were carried out in 20 mM Tris/HCl, 50 mM KCl, 0.1 mM EDTA, and 1 mM NaN_3 at pH 7.4. Supernatants (S_1), supernatants after washing (S_2), and pellets (P) were subjected to SDS−PAGE, and proteins were visualized by Coomassie staining. To unambiguously identify ezrin, a sample of pure protein without vesicles was added. M = molecular-weight marker.

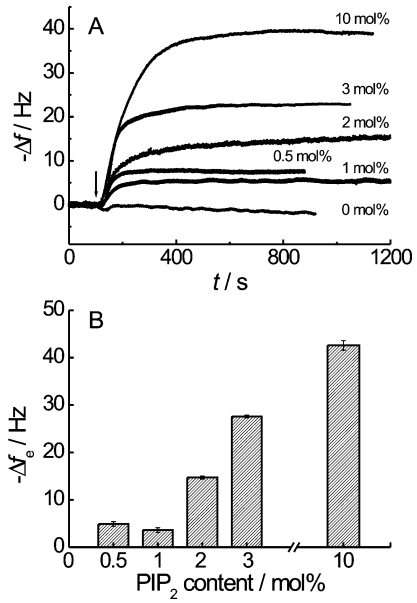

FIGURE 2: (A) Time courses of the frequency shifts upon the addition of 0.1 μM ezrin (arrow) to solid-supported membranes composed of POPC and various amounts of PIP_2 in 20 mM Tris/HCl, 50 mM KCl, 0.1 mM EDTA, and 1 mM NaN_3 at pH 7.4. (B) Mean Δf_e values obtained after the adsorption of 0.1 μM ezrin to solid-supported membranes composed of POPC and various amounts of PIP_2 in 20 mM Tris/HCl, 50 mM KCl, 0.1 mM EDTA, and 1 mM NaN_3 at pH 7.4.

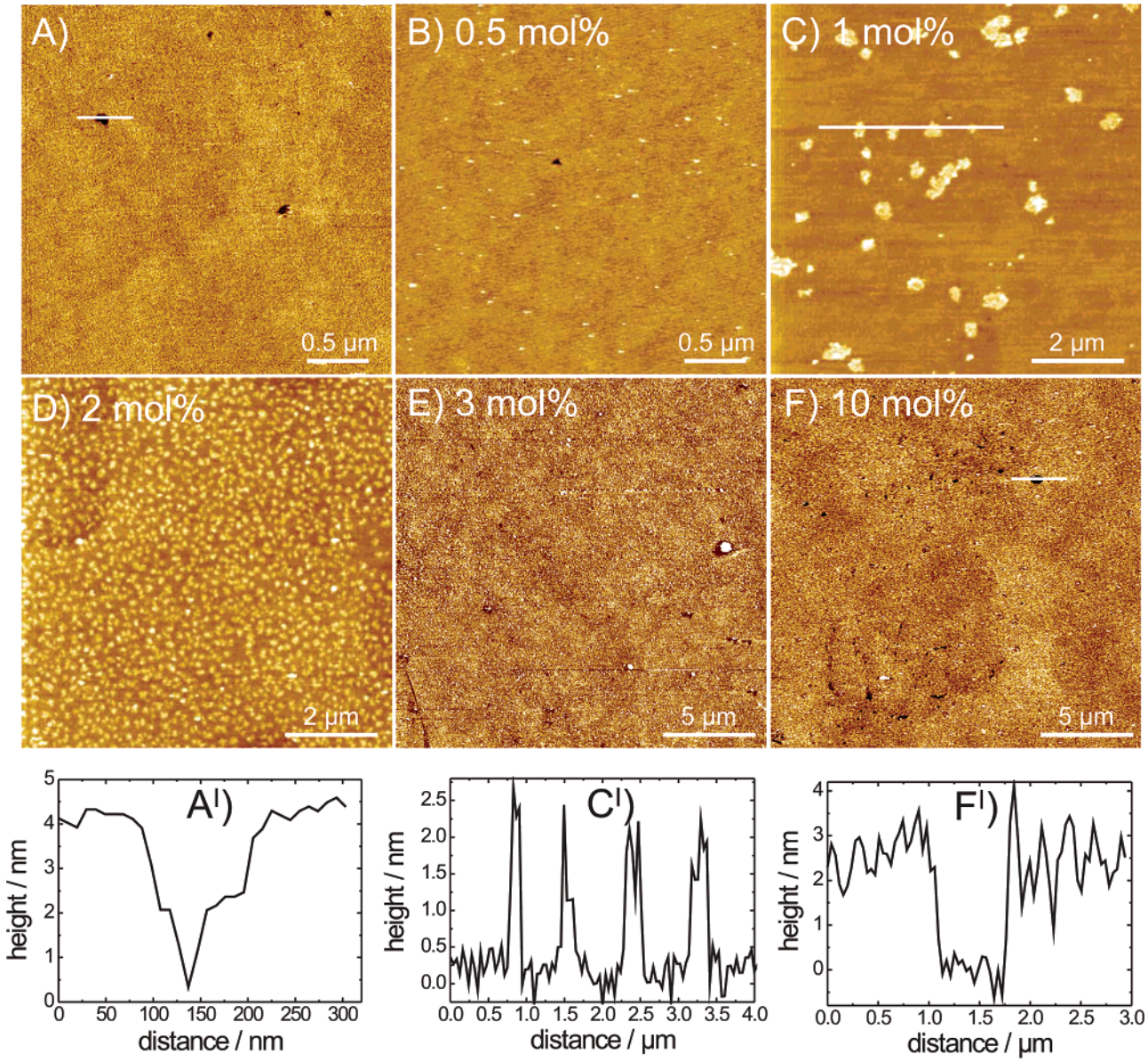

FIGURE 3: SFM images showing the topography (TappingMode) of solid-supported membranes with different amounts of PIP_2 in 20 mM Tris/HCl, 50 mM KCl, 0.1 mM EDTA, and 1 mM NaN_3 at pH 7.4. (A) Membrane containing 3 mol % PIP_2 before the addition of ezrin. (A^I) Cross-section along the line shown in A. Membranes containing (B) 0.5 mol % PIP_2, (C) 1 mol % PIP_2, (D) 2 mol % PIP_2, (E) 3 mol % PIP_2, and (F) 10 mol % PIP_2 after the addition of 1 μM ezrin. In C^I and F^I, the corresponding cross-sections along the lines shown in C and F are presented.

was observed at a PIP_2 concentration of 10 mol %. To keep the PIP_2 concentrations in a physiologically relevant range, we did not investigate concentrations larger than 10 mol %. A reduction of the PIP_2 concentration decreases the resonance frequency shifts, indicating that less protein has been bound to the membrane. A total of 0.5 and 1 mol % PIP_2 in the membrane led to almost the same frequency shift. In the absence of PIP_2, the resonance frequency of the quartz plate was not altered, confirming the specificity of ezrin for the receptor molecule PIP_2. Figure 2B summarizes the maximum frequency shifts as a function of the PIP_2 concentration. The mean $-\Delta f_e$ values after 20 min after protein addition obtained are 42 ± 1 Hz ($n = 3$) for 10 mol % PIP_2, 27.6 ± 0.3 Hz ($n = 7$) for 3 mol % PIP_2, 14.7 ± 0.3 Hz ($n = 6$) for 2 mol % PIP_2, 3.6 ± 0.5 Hz ($n = 5$) for 1 mol % PIP_2, and 4.9 ± 0.5 Hz ($n = 4$) for 0.5 mol % PIP_2.

The question arose of how the protein is arranged on the planar membrane and how the PIP_2 concentration influences the packing of the protein on the surface. To address these questions, we employed SFM. For SFM experiments, vesicles composed of a mixture of POPC and PIP_2 were spread on oxidized silicon wafers. Bilayer formation was analyzed by visualizing the lipid bilayers on the silica substrates by SFM (Figure 3A). A very smooth surface was monitored with no particular features, demonstrating the formation of almost complete bilayers and a homogeneous distribution of the receptor lipids. No domain formation could be observed. In rare cases, small holes were identified as defects of the bilayer, which confirmed the existence of a membrane. A height analysis of these holes showed a depth of 4−5 nm (Figure 3A^I), which is in good accordance with the theoretical height of a lipid bilayer. To obtain this reference value if no defects were present in the prepared lipid bilayer, a scan window was scratched in the bilayer, employing large forces at high scan velocity.

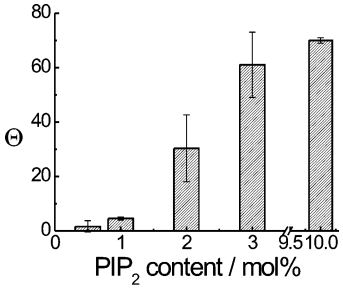

FIGURE 4: Mean values of the protein coverage as obtained from pixel analysis of the SFM images depending upon the PIP_2 content in the solid-supported membranes. The values are averages of at least four images.

The adsorption of protein was initiated by injecting ezrin into the solid-supported membrane at a final concentration of 1 μM. At various adsorption times, SFM images were taken at room temperature. Because the adsorption process is diffusion-limited, coverage increased rather slowly compared to the kinetics monitored by QCM, where the solution was in constant flow. Adsorption was called complete if no further adsorption was observed by SFM. Representative topographic images of membranes after adsorption of ezrin are depicted in parts B−F of Figure 3 as a function of the PIP_2 concentration. At low PIP_2 concentrations, only a small area of the surface is covered by ezrin. Small protein aggregates with a height of 1.8 ± 0.2 nm as deduced from histogram analysis are observed, which are attributed to attractive lateral interactions between ezrin molecules, i.e., positive cooperative binding of ezrin to the membrane. An increase in surface coverage is observed with an increasing PIP_2 concentration, which is in agreement with the QCM results. An almost complete surface coverage was monitored at a PIP_2 concentration of 3 mol %. A further increase in the PIP_2 concentration up to 10 mol % results in a further increased protein coverage, consistent with the QCM results. The formation of a protein monolayer was analyzed by height analysis. The height profile depicted in Figure 3F[I] of an area, where a defect in the protein layer on top of a defect-free lipid bilayer occurs, shows a height difference of ∼2−3 nm, which confirms a monomolecular protein arrangement.

In Figure 4, the protein coverage as obtained by pixel analysis from the topography images is given as a function of the PIP_2 concentration in the membrane. The results are in good agreement with those of the QCM measurements. An almost identical protein coverage at a PIP_2 concentration of 0.5 and 1 mol % in the solid-supported membrane is observed. With an increasing PIP_2 concentration, the surface coverage increases up to a maximum protein coverage of about 70%.

Reversibility of Ezrin Adsorption. As a mediator between the plasma membrane and the cytoskeleton, ezrin appears to play a crucial role in the dynamics of actin formation. To function as such, reversibility of binding is of major importance. We investigated in detail the reversibility of ezrin adsorption and the lateral distribution of proteins after desorption by means of QCM and SFM. Figure 5 shows the time-resolved adsorption and desorption upon the addition of 0.3 μM ezrin as obtained by the QCM technique. The protein was first added to a solid-supported POPC/PIP_2 (97:3) membrane in 20 mM Tris/HCl, 50 mM KCl, 0.1 mM EDTA, and 1 mM NaN_3 at pH 7.4, which resulted in a

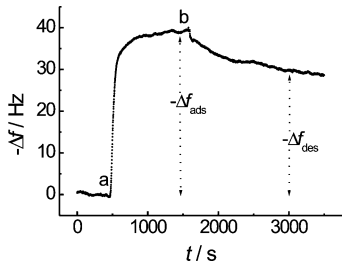

FIGURE 5: Representative time course of the adsorption of ezrin (a) to a solid-supported POPC/PIP_2 (97:3) membrane in 20 mM Tris/HCl, 50 mM KCl, 0.1 mM EDTA, and 1 mM NaN_3 at pH 7.4, followed by desorption of ezrin (b). The frequency shift as a result of protein adsorption is $-\Delta f_{ads} = 39 \pm 1$ Hz for $c_{ezrin} = 0.30$ μM. The final value obtained for desorption is $-\Delta f_{des} = 29 \pm 1$ Hz.

decrease in resonance frequency, indicating a successful adsorption of protein onto the membrane. A total of 1100 s after injection of the protein solution, the system was flushed with pure buffer to initiate ezrin desorption, resulting in an increase in resonance frequency (Figure 5). The observed desorption process indicates that ezrin remains partly bound to the membrane. Interestingly, experiments carried out with the same ezrin concentration show a variable ratio of adsorption to desorption (data not shown). At a given ezrin concentration of 0.1 μM, the obtained frequency shifts at equilibrium varied between 23 and 32 Hz. After the desorption process was initiated by flushing the system with pure buffer solution, the change in resonance frequency varied between 4 and 17 Hz. Because the lipid receptor (PIP_2) is homogeneously distributed and no domain formation occurs in the membrane (see Figure 3A), the "irreversibly" bound protein fraction and its variation as observed in the monitored time period are attributed to a positive cooperative lateral interaction of ezrin molecules on the membrane surface (*36*−*38*), while it is known that ezrin does not form oligomers ($n > 2$) in solution (*37*, *38*). To further elucidate the desorption process, SFM measurements were performed. Figure 6 shows an image of a POPC/PIP_2 (90:10) lipid bilayer on which ezrin had been adsorbed before the specimen was rinsed thoroughly with buffer. Prior to flushing with buffer, the surface was completely covered with protein. After flushing with buffer, some large defect areas with a depth of ∼2 nm are clearly discernible, while most of the protein still remained bound to the surface. Apparently, the protein desorbs preferentially in certain areas, while in others, it remains completely membrane-bound, which might be ascribed to lateral protein−protein interactions increasing the overall affinity of the protein to the membrane considerably. On the basis of the results obtained above, we propose a positive cooperative binding process of ezrin to PIP_2-doped membranes; i.e., attractive lateral protein−protein interactions occur when the protein is bound to the surface. To further confirm this hypothesis, we performed time-elapsed SFM images of a PIP_2-containing membrane after the addition of ezrin. As shown in Figure 7, the ezrin monolayer grows starting from a few nucleation sites, governed by attractive lateral interactions of the proteins on the membrane.

On the basis of these results, we intended to describe the adsorption and desorption kinetics obtained by QCM with a cooperative model developed by Minton (*39*, *40*). Figure 8 shows a schematic drawing of the conceivable kinetic pathways proposed by Minton (*40*). Briefly, the model

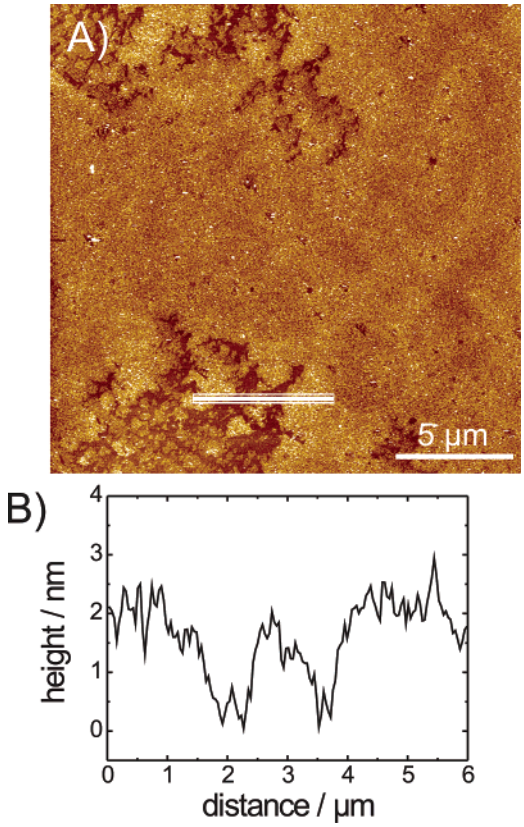

FIGURE 6: (A) SFM image showing the topography (TappingMode) of a solid-supported membrane (10 mol % PIP_2) after the adsorption of ezrin and after rinsing the sample thoroughly with buffer. (B) Cross-section along the line shown in A.

comprises the formation of monolayer surface clusters, which are assumed to grow by the reversible adsorption of protein molecules to pre-existing clusters. We kept the nomenclature as proposed by Minton (*40*). All of the depicted processes can be described through their forward and backward rate constants. In principle, one can distinguish between two pathways of adsorbate cluster growth. In the first case, the soluble protein adsorbs on a vacant surface space at a forward rate constant k_{1f}. T_1 marks the transition state for this initial process. After deposition, the adsorbed protein diffuses to the edge of the protein cluster (k_{2f}) followed by accretion, thus increasing the size of the cluster. T_2 illustrates the transition state for this process. The second process covers the deposition of soluble proteins onto a cluster (k_{3f}) and subsequent insertion into it. In accordance with Minton, this will be called piggyback deposition, and its transition state is illustrated in T_3. The reversibility of the individual processes is expressed by the backward rate constants k_{1b}, k_{2b}, and k_{3b}, respectively.

Adjusting the values for $c^* = K_1^{ads}c$, k_{1b}, U_c, k_{2f}^0, and J, we simulated adsorption and desorption time courses and compared them with the experimental data obtained from the QCM measurements. c^* is an affinity-scaled solution concentration of the protein; $K_1^{ads} = k_{1f}/k_{1b}$ is the thermodynamic equilibrium association constant for adsorption of the protein from solution; c is the concentration of the protein in solution; k_{1b} is the backward rate constant for surface protein desorption; U_c is the potential energy of a single adsorbate−adsorbate contact in the cluster; k_{2f}^0 is the forward rate constant for surface protein addition; and J is a dimensionless constant allowing for piggyback deposition on pre-existing clusters. The higher J, the more likely a piggyback event occurs. We used the circular cluster model that assumes circular footprints of the ezrin clusters with $i = 1-100$ (*39*, *40*). In Figure 9, representative time courses are depicted. The arrows indicate the points of flushing the system with buffer solution. The upper parts of the panels show data points derived from QCM measurements using solid-supported membranes composed of $POPC/PIP_2$ (97:3) in 20 mM Tris/HCl, 50 mM KCl, 0.1 mM EDTA, and 1 mM NaN_3 at pH 7.4. To compare the experimental with the simulated data, it is necessary to translate the frequency readouts from the QCM measurements into surface coverage. This is achieved by the assumption that the maximum surface coverage according to the SFM measurements is 70%, which corresponds to the experimentally obtained maximum frequency shift of 43 Hz. The lower parts of the panels show the simulated data points, which were obtained by varying the above-mentioned parameters c^*, k_{1b}, U_c, k_{2f}^0, and J to obtain the best accordance with our experimental data. The value of U_c was set to $-5RT$ for all shown simulations. A negative value of U_c represents attractive lateral interactions between the proteins, i.e., a positive cooperative binding process. To start with, we did not allow for the pathway of piggyback deposition, and hence, J was set to 0. The variation of the other parameters resulted in the curves shown in parts A and B of Figure 9. The simulated curves are in good accordance with the experimental data, emphasizing that the selected model is suitable to describe the adsorption and desorption processes of ezrin. Sometimes, we observed a "drift" during the adsorption process of ezrin as illustrated in Figure 9C. As indicated by the arrow, the drift could be stopped by flushing the system with buffer solution. In these cases, the experimental data could best be described by allowing the piggyback deposition as a second minor pathway; hence, J was set to a small value of 5×10^{-4}. The result is depicted in the lower part of Figure 9C.

To further validate the selected model, we generated an equilibrium adsorption isotherm by variation of the protein concentration in solution, keeping the other parameters at constant values of $k_{1b} = 9 \times 10^{-4}$ s^{-1}, $k_{2f}^0 = 0.05$ s^{-1}, $K_1^{ads} = 10^8$ M^{-1}, $U_c = -5RT$, and $J = 0$, and compared the isotherm with that obtained by plotting the equilibrium frequency shifts $-\Delta f_e$ of our QCM results obtained at different ezrin concentrations. The adsorption isotherm was monitored using a lipid mixture of $POPC/PIP_2$ (97:3), which reflects the content of PIP_2 in natural membranes (*41*) and is sufficient for high ezrin coverage (see Figure 1).

Figure 10 shows the QCM results of the adsorption isotherm together with the calculated curve using the Minton model. In accordance with our results obtained from the kinetic simulations, we assumed that no piggyback deposition occurs and that the adsorption process of ezrin follows in a cooperative fashion. Importantly, all values of the parameters used for simulating the isotherm are in the same range as those determined by the kinetic simulations. In fact, the equilibrium values were extracted from the simulated kinetics at exactly the same time as the experimental data. Figure 10 shows the experimental data (■) together with simulated equilibrium values (—) underlining that indeed cooperative interactions between the proteins govern the adsorption

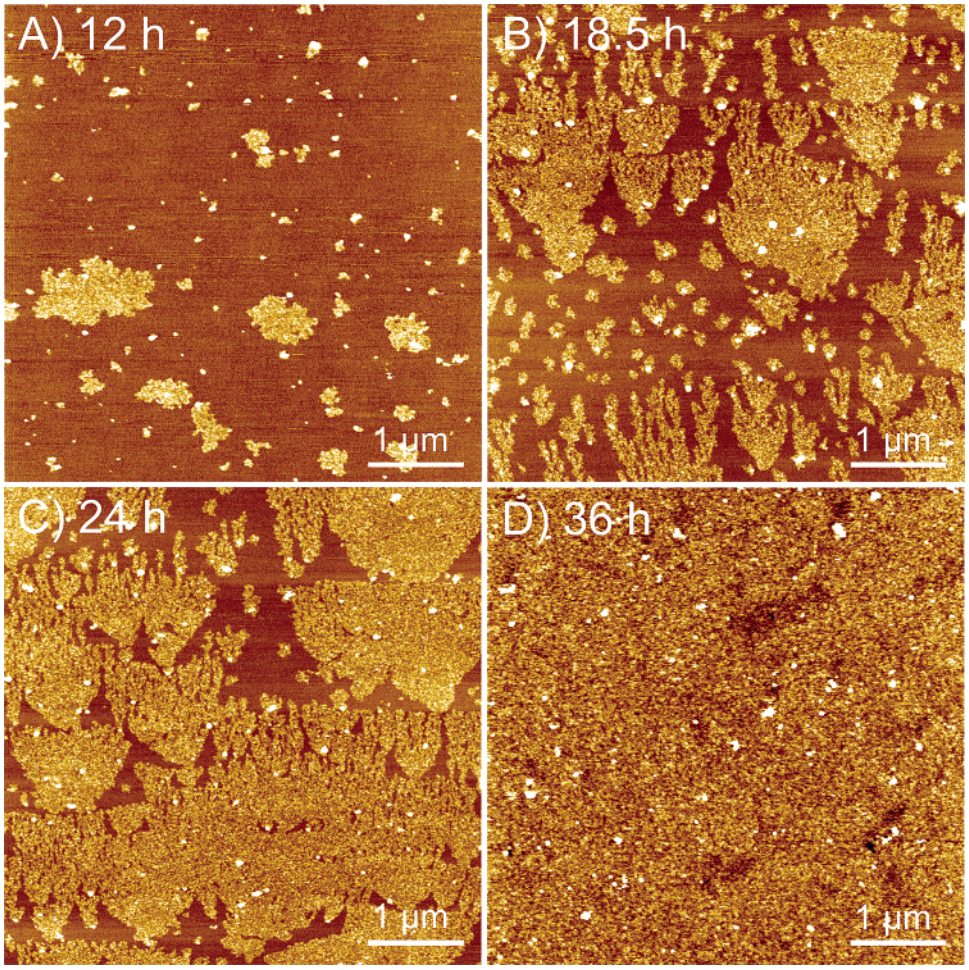

FIGURE 7: Time-elapsed SFM images showing the topography (TappingMode) of a solid-supported membrane (3 mol % PIP_2) after the addition of ezrin. (A) 12 h after the addition of ezrin ($c_{ezrin} = 0.35\ \mu M$) and (B) after 18.5 h, (C) 24 h, and (D) 36 h incubation time with ezrin ($c_{ezrin} = 1.5\ \mu M$).

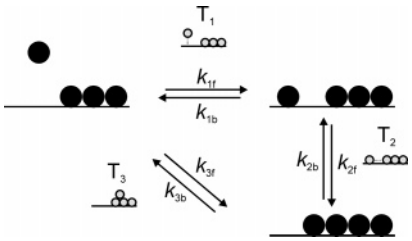

FIGURE 8: Schematic illustration of the kinetic model adapted from Minton (*40*) showing the kinetic pathways and the corresponding transition states. The growth of protein clusters on the surface can either occur through direct deposition (T_1) followed by accretion (T_2) or by piggyback deposition (T_3) and incorporation into the cluster.

process. In conjunction with the SFM measurements, a cooperative adsorption process of ezrin to PIP_2-doped POPC membranes is a highly likely event.

DISCUSSION

By means of the quartz crystal microbalance technique, the interaction of ezrin with PIP_2-containing solid-supported membranes was investigated in detail. The QCM has been proven to be a versatile tool to monitor protein−lipid interactions in a label-free and time-resolved manner (*25*, *26*, *30*). In a first approach, we studied the influence of the PIP_2 concentration in the membrane on ezrin binding. The specificity of the protein for the receptor lipid PIP_2 was demonstrated by a control, in which ezrin was added to a neat POPC membrane and no binding was observable. The amount of bound ezrin increases with increasing PIP_2 concentrations in the membrane, which is in agreement with the vesicle co-sedimentation assays. The sensitivity of the QCM measurements is, however, significantly higher than that of the vesicle co-sedimentation assay. At PIP_2 concentrations of 0.5 and 1 mol %, only negligible binding was detected in the vesicle assays but unambiguous binding was monitored by the QCM experiments.

To gather information about the lateral arrangement of membrane-bound ezrin and its dependence on the PIP_2 content in the membrane, SFM was employed, allowing the visualization of membranes and membrane-bound proteins on a nanometer scale (*28*, *29*, *31*, *32*). POPC membranes containing PIP_2 do not show any particular features but appear rather smooth, indicating a uniform distribution of the lipids, i.e., excluding the formation of membrane domains. Thus, we conclude that PIP_2 does not form lipid domains embedded in a POPC matrix under the conditions chosen. This is in agreement with the results of Denisov et al. (*42*), who monitored a random distribution of acidic lipids in the plane of the membrane by fluorescence microscopy. The addition of ezrin to membranes composed of POPC and 0.5 and 1 mol % PIP_2 results in protein domains with an average height of 1.8 ± 0.2 nm. This is characteristic for

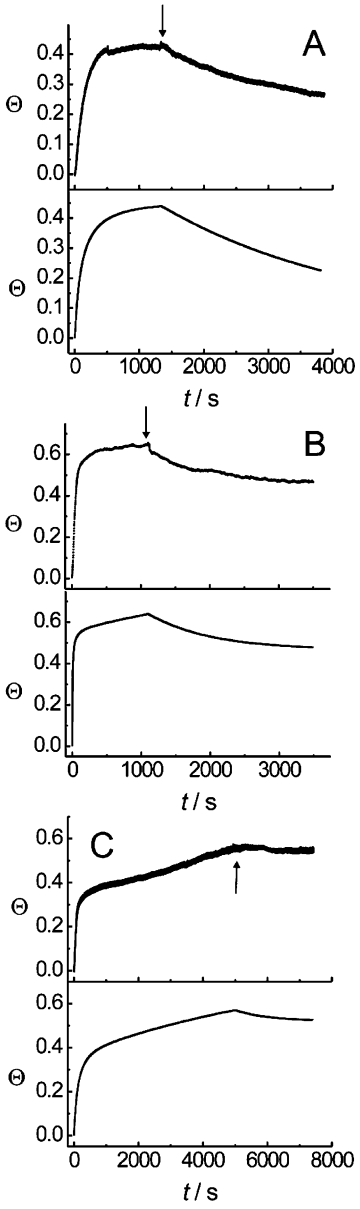

FIGURE 9: Representative time courses of adsorption and desorption of ezrin in comparison with simulated data. The experiments were carried out using solid-supported POPC/PIP_2 (97:3) membranes in 20 mM Tris/HCl, 50 mM KCl, 0.1 mM EDTA, and 1 mM NaN_3 at pH 7.4. The applied ezrin concentrations are (A) $c_{ezrin} = 0.06$ μM, (B) $c_{ezrin} = 0.30$ μM, and (C) $c_{ezrin} = 0.07$ μM. The obtained frequency shifts of the QCM measurements were transformed into protein surface coverage, assuming that the maximum frequency shift of 43 Hz corresponds to a surface coverage of 0.7. The upper part of the panels shows data points derived from QCM measurements, and the lower part of the panels shows the simulated data points. Simulation parameters: $U_c = -5RT$ throughout and (A) $c^* = 13$, $k_{2f}^0 = 0.015$ s^{-1}, $J = 0$, and $k_{1b} = 3.5 \times 10^{-4}$ s^{-1}; (B) $c^* = 200$, $k_{2f}^0 = 0.025$ s^{-1}, $J = 0$, and $k_{1b} = 10 \times 10^{-4}$ s^{-1}; and (C) $c^* = 5$, $k_{2f}^0 = 0.08$ s^{-1}, $J = 5 \times 10^{-4}$, and $k_{1b} = 7 \times 10^{-4}$ s^{-1}.

the formation of ezrin protein clusters bound in a monomolecular fashion. In comparison with a height of approximately 4 nm of the crystalline N-terminal domain of ezrin (*43*), the measured height is about half of that, which may be a result of mechanical deformation caused by the SFM tip (*44*, *45*). The formation of protein clusters is supposed to be a result of lateral protein−protein interactions. The propensity of ezrin to form dimers and oligomers has been reported by

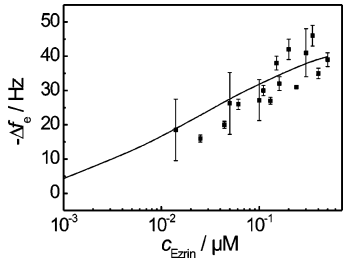

FIGURE 10: Experimental (■) and simulated (−) adsorption isotherm of ezrin, binding to a solid-supported POPC/PIP_2 (97:3) membrane in 20 mM Tris/HCl, 50 mM KCl, 0.1 mM EDTA, and 1 mM NaN_3 at pH 7.4. Simulation parameters: $k_{1b} = 9 \times 10^{-4}$ s^{-1}, $k_{2f}^0 = 0.05$ s^{-1}, $K_1^{ads} = 10^8$ M^{-1}, $U_c = -5RT$, and $J = 0$.

others (*36*−*38*, *46*). Higher ordered adducts of ezrin have been found in extracts of placental microvilli and in gastric parietal cells. In addition, it has been shown that epidermal growth factor (EGF) stimulation of human epidermoid carcinoma cells induces the rapid formation of ezrin oligomers.

The PIP_2-binding motif of ezrin contains several lysine residues, which are crucial for the PIP_2 interaction (*21*). Binding of an ezrin molecule to PIP_2 may induce a recruitment of additional PIP_2 molecules toward the protein, which would result in a PIP_2 depletion of the residual membrane. It has been shown that binding of basic peptides to membranes leads to the formation of lateral domains enriched in PIP_2 (*42*). Because of this process, it is likely that not all PIP_2 molecules are accessible for further ezrin adsorption. At PIP_2 concentrations of 3 mol % and larger, an almost complete coverage of the surface is observed by SFM. If one calculates the surface coverage of ezrin, assuming that one PIP_2 molecule occupies an area of 70 $Å^2$ (*47*) and binds one ezrin molecule, which covers an area of about 5000 $Å^2$ (*43*, *48*), a maximum coverage is expected at a PIP_2 content of 2 mol %. However, the statistical evaluation of the SFM data shows that at a PIP_2 content of 2 mol % the surface coverage is around 30%, which is around half of that expected from the calculation. Besides experimental uncertainties, an explanation for this discrepancy might be found in a preferential localization of PIP_2 molecules underneath an ezrin molecule.

To further investigate the dynamics of the binding process of ezrin to solid-supported membranes composed of POPC/PIP_2 (97:3), we investigated the reversibility of ezrin adsorption by means of QCM and SFM measurements. It appears that upon removing ezrin from solution only part of the ezrin molecules readily desorbs from the membrane, while a significant part of the proteins remains bound to the bilayer. Together with the SFM results demonstrating the formation of protein clusters upon adsorption, we propose that a positive cooperative binding of ezrin, i.e., occurrence of lateral protein−protein interactions, is responsible for the observations. On the basis of our findings, we attempted to model the kinetics and thermodynamics of ezrin adsorption by employing a kinetic model developed by Minton (*39*, *40*). The model includes the formation and subsequent growth of monolayer surface clusters of adsorbed molecules. Using this model, it was possible to generate adsorption and desorption curves that reproduce those monitored by means of QCM, supporting the idea of a positive cooperative binding of ezrin to PIP_2-containing lipid bilayers. In par-

ticular, it was demonstrated that the partial "pseudo-irreversible" binding behavior is a result of the positive cooperative binding of ezrin. Noteworthy, it was not possible to use a Langmuirian kinetic to describe the data properly. It was moreover found that permitting piggyback deposition of ezrin on pre-existing clusters may account for the slowly evolving second time-dependent increase in surface coverage that was sometimes observed in the kinetic curves at higher coverage. Many examples are found in the literature, where positive cooperativity is described in surface biochemistry. For instance, it has been reported for annexin A5 binding to supported lipid bilayers (*30*), for the adsorption of lysozyme onto $Si(Ti)O_2$ surfaces (*49*), for the adsorption of ferritin and fibrinogen onto hydrophilic and hydrophobic silicon surfaces (*50*), and even for antigen−antibody interactions (*51*).

Not only the binding kinetics but also the equilibrium coverage for various ezrin concentrations reconstructed with the kinetic Minton model are very similar to those obtained from QCM measurements, revealing that the intrinsic adsorption constant K_1^{ads} of ezrin binding to PIP_2 in the absence of lateral protein interactions amounts to 10^8 M^{-1}. Because the adsorption isotherm has been reconstructed from kinetic data and not by an equilibrium model based on the scaled particle theory (*52*), one has to be aware of the fact that the extracted data are not truly equilibrium values.

In summary, we propose a model in which PIP_2 is uniformly distributed in a solid-supported POPC membrane and interacts with high specificity with ezrin, resulting in a cooperative adsorption of an ezrin monolayer to the surface. The interaction with PIP_2 may result in a (partial) activation of ezrin that could help to establish a cooperative lateral interaction between ezrin molecules. In particular, only ezrin clusters might play an important role in connecting F-actin with the membrane.

ACKNOWLEDGMENT

We are very grateful to Allen P. Minton for providing us with his Matlab code to simulate the presented data.

REFERENCES

1. Bretscher, A., Edwards, K., and Fehon, R. G. (2002) ERM proteins and merlin: Integrators at the cell cortex, *Nat. Rev. Mol. Cell Biol. 3*, 586−599.
2. Mangeat, P., Roy, C., and Martin, M. (1999) ERM proteins in cell adhesion and membrane dynamics, *Trends Cell Biol. 9*, 187−192.
3. Tsukita, S., and Yonemura, S. (1999) Cortical actin organization: Lessons from ERM (ezrin/radixin/moesin) proteins, *J. Biol. Chem. 274*, 34507−34510.
4. Polesello, C., and Payre, F. (2004) Small is beautiful: What flies tell us about ERM protein function in development, *Trends Cell Biol. 14*, 294−302.
5. Turunen, O., Wahlstrom, T., and Vaheri, A. (1994) Ezrin has a COOH-terminal actin-binding site that is conserved in the ezrin protein family, *J. Cell Biol. 126*, 1445−1453.
6. Bretscher, A. (1983) Purification of an 80,000-dalton protein that is a component of the isolated microvillus cytoskeleton, and its localization in nonmuscle cells, *J. Cell Biol. 97*, 425−432.
7. Gould, K. L., Bretscher, A., Esch, F. S., and Hunter, T. (1989) cDNA cloning and sequencing of the protein−tyrosine kinase substrate, ezrin, reveals homology to band 4.1, *EMBO J. 8*, 4133−4142.
8. Reczek, D., and Bretscher, A. (1998) The carboxyl-terminal region of EBP50 binds to a site in the amino-terminal domain of ezrin that is masked in the dormant molecule, *J. Biol. Chem. 273*, 18452−18458.
9. Tsukita, S., Oishi, K., Sato, N., Sagara, J., and Kawai, A. (1994) ERM family members as molecular linkers between the cell surface glycoprotein CD44 and actin-based cytoskeletons, *J. Cell Biol. 126*, 391−401.
10. Yonemura, S., Hirao, M., Doi, Y., Takahashi, N., Kondo, T., and Tsukita, S. (1998) Ezrin/radixin/moesin (ERM) proteins bind to a positively charged amino acid cluster in the juxta-membrane cytoplasmic domain of CD44, CD43, and ICAM-2, *J. Cell Biol. 140*, 885−895.
11. Legg, J. W., and Isacke, C. M. (1998) Identification and functional analysis of the ezrin-binding site in the hyaluronan receptor, CD44, *Curr. Biol. 8*, 705−708.
12. Heiska, L., Alfthan, K., Gronholm, M., Vilja, P., Vaheri, A., and Carpen, O. (1998) Association of ezrin with intercellular adhesion molecule-1 and -2 (ICAM-1 and ICAM-2). Regulation by phosphatidylinositol 4,5-bisphosphate, *J. Biol. Chem. 273*, 21893−21900.
13. Niggli, V., Andreoli, C., Roy, C., and Mangeat, P. (1995) Identification of a phosphatidylinositol-4,5-bisphosphate-binding domain in the N-terminal region of ezrin, *FEBS Lett. 376*, 172−176.
14. Hirao, M., Sato, N., Kondo, T., Yonemura, S., Monden, M., Sasaki, T., Takai, Y., and Tsukita, S. (1996) Regulation mechanism of ERM (ezrin/radixin/moesin) protein/plasma membrane association: Possible involvement of phosphatidylinositol turnover and Rho-dependent signaling pathway, *J. Cell Biol. 135*, 37−51.
15. Fievet, B. T., Gautreau, A., Roy, C., Del Maestro, L., Mangeat, P., Louvard, D., and Arpin, M. (2004) Phosphoinositide binding and phosphorylation act sequentially in the activation mechanism of ezrin, *J. Cell Biol. 164*, 653−659.
16. Yonemura, S., Matsui, T., and Tsukita, S. (2002) Rho-dependent and -independent activation mechanisms of ezrin/radixin/moesin proteins: An essential role for polyphosphoinositides in vivo, *J. Cell Sci. 115*, 2569−2580.
17. Divecha, N., and Irvine, R. F. (1995) Phospholipid signaling, *Cell 80*, 269−278.
18. Janmey, P. A. (1994) Phosphoinositides and calcium as regulators of cellular actin assembly and disassembly, *Annu. Rev. Physiol. 56*, 169−191.
19. Martin, T. F. (2001) PI(4,5)P(2) regulation of surface membrane traffic, *Curr. Opin. Cell Biol. 13*, 493−499.
20. McLaughlin, S., Wang, J., Gambhir, A., and Murray, D. (2002) PIP_2 and proteins: Interactions, organization, and information flow, *Annu. Rev. Biophys. Biomol. Struct. 31*, 151−175.
21. Barret, C., Roy, C., Montcourrier, P., Mangeat, P., and Niggli, V. (2000) Mutagenesis of the phosphatidylinositol 4,5-bisphosphate (PIP_2) binding site in the NH_2-terminal domain of ezrin correlates with its altered cellular distribution, *J. Cell Biol. 151*, 1067−1080.
22. Bretscher, A., Chambers, D., Nguyen, R., and Reczek, D. (2000) ERM-Merlin and EBP50 protein families in plasma membrane organization and function, *Annu. Rev. Cell Dev. Biol. 16*, 113−143.
23. Simons, P. C., Pietromonaco, S. F., Reczek, D., Bretscher, A., and Elias, L. (1998) C-Terminal threonine phosphorylation activates ERM proteins to link the cell's cortical lipid bilayer to the cytoskeleton, *Biochem. Biophys. Res. Commun. 253*, 561−565.
24. Koltzscher, M., Neumann, C., Konig, S., and Gerke, V. (2003) Ca^{2+}-Dependent binding and activation of dormant ezrin by dimeric S100P, *Mol. Biol. Cell 14*, 2372−2384.
25. Janshoff, A., Galla, H. J., and Steinem, C. (2000) Piezoelectric mass-sensing devices as biosensors−An alternative to optical biosensors? *Angew. Chem., Int. Ed. 39*, 4004−4032.
26. Janshoff, A., and Steinem, C. (2001) Quartz crystal microbalance for bioanalytical applications, *Sens. Update 9*, 313−354.
27. Richter, R. P., Berat, R., and Brisson, A. R. (2006) Formation of solid-supported lipid bilayers: An integrated view, *Langmuir 22*, 3497−3505.
28. Richter, R. P., and Brisson, A. (2004) QCM-D on mica for parallel QCM-D−AFM studies, *Langmuir 20*, 4609−4613.
29. Richter, R. P., and Brisson, A. R. (2005) Following the formation of supported lipid bilayers on mica: A study combining AFM, QCM-D, and ellipsometry, *Biophys. J. 88*, 3422−3433.
30. Richter, R. P., Him, J. L., Tessier, B., Tessier, C., and Brisson, A. R. (2005) On the kinetics of adsorption and two-dimensional self-assembly of annexin A5 on supported lipid bilayers, *Biophys. J. 89*, 3372−3385.

31. Dufrene, Y. F., and Lee, G. U. (2000) Advances in the characterization of supported lipid films with the atomic force microscope, *Biochim. Biophys. Acta 1509*, 14−41.
32. Janshoff, A., and Steinem, C. (2001) Scanning force microscopy of artificial membranes, *ChemBioChem 2*, 798−808.
33. Bradford, M. M. (1976) A rapid and sensitive method for the quantitation of microgram quantities of protein utilizing the principle of protein−dye binding, *Anal. Biochem. 72*, 248−254.
34. Laemmli, U. K. (1970) Cleavage of structural proteins during the assembly of the head of bacteriophage T4, *Nature 227*, 680−685.
35. Kastl, K., Ross, M., Gerke, V., and Steinem, C. (2002) Kinetics and thermodynamics of annexin A1 binding to solid-supported membranes: A QCM study, *Biochemistry 41*, 10087−10094.
36. Berryman, M., Gary, R., and Bretscher, A. (1995) Ezrin oligomers are major cytoskeletal components of placental microvilli: A proposal for their involvement in cortical morphogenesis, *J. Cell Biol. 131*, 1231−1242.
37. Bretscher, A., Gary, R., and Berryman, M. (1995) Soluble ezrin purified from placenta exists as stable monomers and elongated dimers with masked C-terminal ezrin−radixin−moesin association domains, *Biochemistry 34*, 16830−16837.
38. Chambers, D. N., and Bretscher, A. (2005) Ezrin mutants affecting dimerization and activation, *Biochemistry 44*, 3926−3932.
39. Minton, A. P. (2000) Effects of excluded surface area and adsorbate clustering on surface adsorption of proteins I. Equilibrium models, *Biophys. Chem. 86*, 239−247.
40. Minton, A. P. (2001) Effects of excluded surface area and adsorbate clustering on surface adsorption of proteins. II. Kinetic models, *Biophys. J. 80*, 1641−1648.
41. Zachowski, A. (1993) Phospholipids in animal eukaryotic membranes: Transverse asymmetry and movement, *Biochem. J. 294* (part 1), 1−14.
42. Denisov, G., Wanaski, S., Luan, P., Glaser, M., and McLaughlin, S. (1998) Binding of basic peptides to membranes produces lateral domains enriched in the acidic lipids phosphatidylserine and phosphatidylinositol 4,5-bisphosphate: An electrostatic model and experimental results, *Biophys. J. 74*, 731−744.
43. Smith, W. J., Nassar, N., Bretscher, A., Cerione, R. A., and Karplus, P. A. (2003) Structure of the active N-terminal domain of ezrin. Conformational and mobility changes identify keystone interactions, *J. Biol. Chem. 278*, 4949−4956.
44. Bayburt, T. H., Carlson, J. W., and Sligar, S. G. (2000) Single molecule height measurements on a membrane protein in nanometer-scale phospholipid bilayer disks, *Langmuir 16*, 5993−5997.
45. Menke, M., Gerke, V., and Steinem, C. (2005) Phosphatidylserine membrane domain clustering induced by annexin A2/S100A10 heterotetramer, *Biochemistry 44*, 15296−15303.
46. Zhu, L., Liu, Y., and Forte, J. G. (2005) Ezrin oligomers are the membrane-bound dormant form in gastric parietal cells, *Am. J. Physiol. Cell Physiol. 288*, C1242−C1254.
47. Nagle, J. F., and Tristram-Nagle, S. (2000) Structure of lipid bilayers, *Biochim. Biophys. Acta 1469*, 159−195.
48. Hamada, K., Shimizu, T., Matsui, T., Tsukita, S., Tsukita, S., and Hakoshima, T. (2000) Structural basis of the membrane-targeting and unmasking mechanisms of the radixin FERM domain, *EMBO J. 19*, 4449−4462.
49. Ball, V., and Ramsden, J. J. (1997) Absence of surface exclusion in the first stage of lysozyme adsorption is driven through electrostatic self-assembly, *J. Phys. Chem. B 101*, 5465−5469.
50. Nygren, H., Alaeddin, S., Lundstroem, I., and Magnusson, K. E. (1994) Effect of surface wettability on protein adsorption and lateral diffusion. Analysis of data and a statistical model, *Biophys. Chem. 49*, 263−272.
51. Nygren, H. (1994) Kinetics of antibody binding to surface-immobilized antigen. Analysis of data and an empiric model, *Biophys. Chem. 52*, 45−50.
52. Minton, A. P. (1996) Adsorption of globular proteins on locally planar surfaces: Models for the effect of excluded surface area and aggregation of adsorbed protein on adsorption equilibria, *Biophys. J. 71*, 2367−2374.

BI061064A